

Area-preserving Mesh Parameterization for Poly-Annulus Surfaces Based on Optimal Mass Transportation

Kehua Su^a, Li Cui^{b,*}, Kun Qian^{c,g}, Na Lei^d, Junwei Zhang^e, Min Zhang^f, Xianfeng David Gu^g

^a*State Key Laboratory of Software Engineering, Wuhan University, Wuhan, China*

^b*School of Mathematical Science, Beijing Normal University, Beijing, China*

^c*School of Civil Engineering and Mechanics, Kunming University of Science and Technology, Kunming, China*

^d*School of Software, Dalian University of Technology, Dalian, China*

^e*Stony Brook University, Stony Brook, New York, USA*

^f*Center of mathematical sciences and applications, Harvard University, Boston, USA*

^g*Computer Science Department, Stony Brook University, Stony Brook, New York, USA*

Abstract

This work proposes a novel method for computing area-preserving parameterization for genus zero surfaces with multiple boundaries (poly-annuli), which is based on discrete optimal mass transportation and surface Ricci Flow. We first begin with a conformal mapping (which may greatly distort area) by Ricci Flow and then correct the area distortion using the mass transport procedure via a convex optimization. The method is intrinsic and stable, and the resulting parameterization preserves area element and minimizes angle distortion. Comparing with existing algorithms, our method is more general and flexible. It can handle surfaces with more complicated topology, and gives users full control of the target measure, such as the areas of the holes. We have tested the method for applications in various fields. Our experimental results demonstrate the efficiency and efficacy of the proposed method.

Keywords: Area-preservation mapping, multi-holed surface, surface flattening,

*Corresponding author

Email addresses: skhemailg@gmail.com (Kehua Su), licui@bnu.edu.cn (Li Cui), qiankun630@gmail.com (Kun Qian), nalei@outlook.com (Na Lei), junwei.zhang@stonybrook.edu (Junwei Zhang), mzhang@math.harvard.edu (Min Zhang), gu@cs.stonybrook.edu (Xianfeng David Gu)

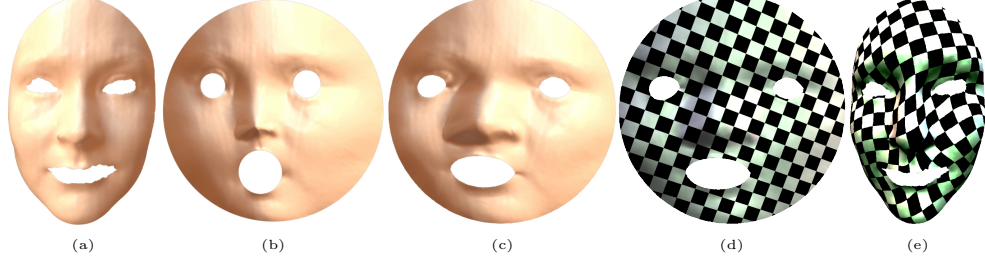


Figure 1: Area-preserving texture mapping for poly-annulus surface. (a)Original 3D poly-annulus surface; (b)Flatting the 3D surface to 2D poly-annulus by Ricci Flow; (c)Area preserving mapping surface by discrete optimal mass transportation(OMT); (d)Casting a checker board texture to(c); (e)The pull-back texture mapping on 3D original surface; (d) and (e) are bijective area preserving texture mapping.

1. Introduction

1.1. Parameterization

Surface parameterization[1][2] refers to the process of mapping a surface embedded in \mathbb{R}^3 to a canonical planar domain with minimal distortions, which has been utilized for a wide variety of applications[3] like remeshing[4][5][6], texture mapping[7][8][9], morphing[10], and shape modelling[11][12][13][14].

In general, distortions can be classified to angle distortion and area distortion. If a parameterization has neither angle distortion nor area distortion, then it must be an isometric mapping, hence preserves Gaussian curvatures. In general, isometric mapping between a 3D surface and a planar domain doesn't exist. Therefore, in practice, research efforts focus on pursuing either angle-preserving parameterizaitons or area-preserving parameterizations.

1.2. Angle-Preserving Parameterization

Angle-preserving parameterizations preserve local shapes, therefore it is highly desirable for practical applications, such as texture mapping, visualization.

Therefore, most existing algorithms emphasize on angle-preserving parameterizations. Many prominent approaches, such as conformal mapping, harmonic mapping and Ricci Flow that attempt to rigorously minimize the angular distortion have been introduced into the computer graphics community.

The angle-preserving mapping may bring huge area distortions in certain surfaces, for example, Figure 2 (b) shows large shrinkage of the lid of the world cup model. In fact, if one wants to conformally map a cylinder onto a planar annulus, the area distortion on the top is exponential with respect to the height of the cylinder. In turn, such distortions usually introduce much difficulty for the downstream texture mapping and model processing. The exponential shrinkage makes the surface registration highly inaccurate, the geometric computation numerically unstable. In order to enlarge the insufficient texture area caused by the parameterization, topological surgeries need to be introduced, which makes the algorithm more complicated and less automatic.

1.3. Area-Preserving Parameterization

Another surface parameterization approach is to minimize the area distortion. The most popular methods include quasi-area parameterization, Lie advection method and optimal mass transportation map method.

Quasi-Area parameterization. A simple and fast method for generating low-stretch mesh parameterizations is shown in [15].

Given a parameterized triangle mesh $M \in \mathbf{R}^3$, consider a mesh triangle $T \in M$ and its corresponding triangle U in the parametric plane \mathbf{R}^2 . The correspondence between the vertices of T and U uniquely defines an affine mapping $P : U \rightarrow T$.

Define, quantity $\sigma(U) = \sqrt{(\Gamma^2 + \gamma^2)/2}$ characterizes the stretch of mapping P , where Γ and γ are the maximal and minimal eigenvalues of the metric tensor induced by the mapping P . For each vertex u_i in the parameter domain, its stretch $\sigma(u_i)$ is defined by

$$\sigma(u_i) = \sqrt{\sum A(T_j) \sigma(U_j)^2 / \sum A(T_j)}.$$

where $A(T)$ denotes the area of triangle T and the sums are taken over all triangles T_j surrounding mesh vertex p_i corresponding to u_i .

For each inner vertex $p_i \in M$ its corresponding vertex $u_i \in \mathbf{R}^2$, minimizes the local quadratic energy

$$E(u_i) = \sum_j w_{ij}(u_j - u_i)^2,$$

where u_j are vertices corresponding to the mesh one-link neighbors of p_i and w_{ij} are positive weights. The optimal positions for u_i are found by solving a sparse system of linear equations

$$\sum_j w_{ij}(u_j - u_i) = 0.$$

Using the local stretch $\sigma(u_i)$ for each inner vertex u_i in the parametric plane to estimate the weight w_{ij} by assigning

$$w_{ij}^{new} = w_{ij}^{old} / \sigma(u_j).$$

The optimization is achieved by minimizing a weighted quadratic energy with positive weights chosen to minimize the parameterization stretch. The quasi-area parameter is fast since it is based on solving a sparse system of linear equations. In contrast, our method has solid mathematical foundation. Our experimental results demonstrate that our method outperforms this method.

Lie Advection. The method in [16] is based on Lie derivative and Cartan's formula. Given a surface S , the Lie advection method designs a time-variant tangent vector field on the surface $\mathbf{v}(t)$, each point $p \in S$ moves on the surface, at the time t the velocity vector of p is $\mathbf{v}(p, t)$. Therefore, we obtain a single-parameter family of diffeomorphisms $\varphi_t : S \rightarrow S$, such that

$$\frac{d}{dt} \varphi_t(p) = \mathbf{v}(p, t).$$

Suppose the area element on the surface is ω , the mapping φ_t induces the pull-back area element, denoted as $\varphi_t^* \omega$, then by Cartan's formula, the Lie derivative of ω

$$\mathcal{L}_{\mathbf{v}} \omega = \frac{d}{dt} \varphi_t^* \omega = i_{\mathbf{v}} d\omega + d(i_{\mathbf{v}} \omega) = d(i_{\mathbf{v}} \omega),$$

where the inner product of \mathbf{v} and the 2-form ω is a 1-form, $i_{\mathbf{v}}\omega = \omega(\mathbf{v}, \cdot)$. One can design the Lie derivative of ω to deform the current area element to the desired one, which is controlled by the vector field $\mathbf{v}(t)$. Therefore, by designing the vector field, one can manipulate the evolution of the area element. This method can handle surfaces with complicated topologies, incorporating landmark constraints. The method has some disadvantages: the solution is not unique, and the iterative procedure of designing time variant vector field is indirect and less efficient.

Optimal Mass Transportation (OMT). Another approach to area-preserving parameterization is based on optimal mass transportation, which is also known as the “earth mover’s problem” [17][7]. Suppose (X, μ) and (Y, ν) are two domains in the Euclidean space with measures μ and ν respectively, $\varphi : X \rightarrow Y$ is a diffeomorphism. We say φ is *measure preserving*, if for any Borel set $B \subset Y$, we have

$$\int_B \nu = \int_{\varphi^{-1}(B)} \mu,$$

equivalently, the PDE is given by

$$\mu = J_\varphi \nu \circ \varphi \tag{1}$$

where J_φ is the Jacobian of the mapping φ . The *Optimal Mass Transportation map* is a measure-preserving mapping, that minimizes the total transportation cost, namely,

$$\begin{aligned} & \min_{\varphi} \int_S c(p, \varphi(p)) \mu(p) dp \\ & \text{s.t.} \\ & \mu = J_\varphi \nu \circ \varphi \end{aligned}$$

where $c(p, q)$ is the transportation cost for moving one unit mass from p to q . There are mainly two approaches to solve OMT problem: one is Kontarovich’s approach [18], and the other is Brenier’s approach [19].

Kontarovich’s approach discretizes both the source and the target as point sets with Dirac measures, $\{(p_1, \mu_1), \dots, (p_m, \mu_m)\}$ and $\{(q_1, \nu_1), \dots, (q_n, \nu_n)\}$

respectively, such that $\sum_{i=1}^m \mu_i = \sum_{j=1}^n \nu_j$, a transportation plan can be represented as $\{\lambda_{ij}\}$, which means the mass λ_{ij} is moved from p_i to q_j , then the optimal mass transportation plan is a linear programming problem:

$$\begin{aligned} & \min_{\lambda} \sum_{i=1}^m \sum_{j=1}^n \lambda_{ij} c(p_i, p_j), \\ & \text{s.t.} \\ & \sum_i \lambda_{ij} = \mu_i, \sum_j \lambda_{ij} = \nu_j. \end{aligned}$$

This method has $O(mn)$ unknowns, and the solution mapping is not as smooth as those obtained by the alternative methods.

Brenier[19] observes that if the cost function $c(p, q)$ is the quadratic Euclidean distance $c(p, q) = |p - q|^2$, then there exists a convex function $u : S \rightarrow \mathbb{R}$, such that the optimal mass transportation map is given by the gradient map of u , $p \rightarrow \nabla u(p)$. In this case, the measure-preserving condition in Eqn. 1 becomes Monge-Ampère equation,

$$\det \left(\frac{\partial^2 u}{\partial x_i \partial x_j} \right) \nu \circ \nabla u = \mu.$$

The discrete OMT method discretizes the target as a point set with Dirac measures with only $O(n)$ unkowns. This method is equivalent to a convex optimization process, which can be achieved using more efficient Newton's method, and the solution is unique.

Our Approach. Most existing optimal mass transportation method can only handle simply connected surfaces. An efficient method to compute area-preserving parameterizations for surfaces with complex topologies is highly advantageous for texture mapping and visualization in research area. In our current work, we propose a novel area-preserving parameterization algorithm, which is based on discrete optimal mass transportation [17] theory, and therefore it is equivalent to a convex optimization, with a unique solution. Furthermore, it is capable of handling genus zero surfaces with multiple boundaries (topological annuli).

Our method is as follows: first, the input topological annulus (S, \mathbf{g}) is conformally mapped onto a circle domain $\varphi : (S, \mathbf{g}) \rightarrow (\Omega, dz d\bar{z})$ using discrete

Ricci flow method [20], where

$$\Omega = \mathbb{D} \setminus \bigcup_{i=1}^k B(p_i, r_i),$$

and $B(p_i, r_i)$ is the disk centered at p_i with radius r_i . Because φ is conformal, the original Riemannian metric on the surface $\mathbf{g} = e^{2\lambda}(dx^2 + dy^2)$. On the unit disk, we define a measure $\mu : \mathbb{D} \rightarrow \mathbb{R}$,

$$\mu(p) = \begin{cases} ae^{2\lambda(p)}, & p \in \Omega \\ b, & p \notin \Omega \end{cases},$$

where a, b are two adjustable constants, such that $\int_{\mathbb{D}} \mu dx dy = \pi$. Then we compute the unique optimal mass transportation map $\tau : (\mathbb{D}, \mu dx \wedge dy) \rightarrow (\mathbb{D}, dx \wedge dy)$. The composition $\tau \circ \phi : (S, \mathbf{g}) \rightarrow \mathbb{D}$ is the desired area-preserving parameterization.

1.4. Previous Work

Conformal Parameterization. The literature for conformal mesh parameterization is vast, and a complete review is beyond the scope of the current work. We refer readers to the thorough surveys [13], [3] and [2]. Many existing parameterizations focus on minimizing angle distortion, such as the method based on Riemann-Cauchy equation [9], harmonic energy minimization [21], holomorphic differentials [22], most isometric parameterizations (MIPS) [23], angle-based flattening [24], conformal equivalence meshes [25], curvature flows [26], conformal equivalence [25], spin transformation [27] and so on.

Locally Injective and Bounded Distortion Mappings. Schüller et al. [28] modify any deformation energy to guarantee a locally injective mapping. Levi and Zorin prioritize higher distortion for minimization and provide a minimal L_∞ -norm solution for distortion control [29]. Fu et al. introduce an advanced MIPS method that inherits the local injectivity of MIPS, achieves as low as possible distortions with high efficiency. Their method depends on an enhanced MIPS energy function that penalizes the maximal distortion and distributes the

distortion evenly, and the inexact block coordinate descent method that avoids local optima.

Lipman et al. [30, 31, 32, 33] propose to construct a maximal convex subspace is the continuous piecewise linear mapping space for bounding the maximal distortion and ensuring no inverted mesh elements. Locally injective mapping with bounded distortion is guaranteed when the algorithms converge. The algorithm is iterative, a quadratic programming or semidefinite programming problem needs to solve at each step. A feasible solution space may not exist if the convex subspace is empty or the upper bound of distortion is too small. In contrast, our method has theoretical advantages that the solution exists and is unique, the algorithm converges to the unique global optimum.

Optimal Mass Transport.

(a). *Monge-Kantorovich.* For optimal mass transport, some approaches based on Monge-Kantorovich theory have been proposed. Zhu et al. [34] applied optimal mass transport for flattening blood vessel in an area preserving mapping for medical visualization. Haker et al. [35] proposed to use optimal mass transport for image registration and warping, the method is parameter free and has the unique global optimum. Dominitz and Tannenbaum [7] proposed to use optimal mass transport for texture mapping. The method first starts with an angle-preserving mapping and then refines the mapping using the mass transport procedure derived via gradient flow. Rehman et al. [36] presented a method for 3D image registration based on optimal mass transport problem. Meanwhile, they stress the fact that the optimization of OMT is computationally expensive and emphasize that it is important to find efficient numerical methods to solve this issue, and it is crucial to extend the results to 3D surfaces.

(b). *Monge-Brenier.* There are also some works based on Monge-Brenier theory. Su et al. proposed an area-preserving mapping method for brain morphological study. Zhao et al. proposed an OMT based method for visualization in [37].

But these methods can only compute the maps from the unit disk domain with Euclidean measure to another disk with general measure.

Merigot [38] has proposed a multi-scale approach to solve optimal transport problem. de Goes et al. [39] have provided an optimal-transport driven approach for 2D shape reconstruction and simplification. Recently they have presented a formulation of capacity-constrained Voronoi tessellation as an optimal transport problem for image processing [40]. This method produces high-quality blue noise point sets with improved spectral and spatial properties.

1.5. Contribution

In summary, the current work has the following contributions:

- This work offers an area-preserving surface parameterization method that is able to handle complicated topologies, such as genus zero surfaces with multiple boundaries.
- The mapping is diffeomorphic and unique under normalization. Moreover, the mapping is invariant under conformal transformations.
- Comparing to existing approaches based on Monge-Kantorovich theory, our method reduces the number of unknown variables from $O(n^2)$ to $O(n)$.

The outline of the remainder of this paper is as follows: In Section 2, we demonstrate the theoretical foundation of Ricci Flow and optimal mass transportation. In Section 3, we discuss some relevant implementation issues. In Section 4, we give some illustrative examples of our scheme, and present an evaluation of the running time and distortion measures of our method, compare with stretch minimization method [15]. Finally, in Section 5, we summarize our work and give some possible future research directions.

2. Theoretical Foundation

In this section, we briefly introduce the theoretic foundations of the current work. We refer readers to more thorough treatments on Ricci flow [41] and Optimal mass transportation theory [17].

2.1. Conformal mapping using Ricci Flow

According to conformal geometry theory, we know that a genus zero surface with multiple boundaries can be conformally mapped onto a planar circle domain[42], the unit disk with circular disks removed. Furthermore, such kind of mapping is unique upto a Möbius transformation, the centers and the radii of inner circles are automatically determined by the geometry of the surface. The so-called generalized Koebe's iteration method is given in [43], which is based on the surface Ricci flow.

Smooth Surface Ricci Flow. Suppose (S, \mathbf{g}) is a surface with several boundaries embedded in \mathbb{R}^3 , g is the natural induced Euclidean metric $\mathbf{g} = (g_{ij})$. We select one boundary as the exterior boundary, the others as the interior boundaries. Let the mapping $\phi : (S, \mathbf{g}) \rightarrow (\Omega, dx^2 + dy^2)$ transform the surface to the planar circle domain Ω , where $dx^2 + dy^2$ is the planar Euclidean metric. We say ϕ is a conformal mapping, or angle-preservation mapping, if ϕ is a diffeomorphism, such that:

$$g(x, y) = e^{2\lambda(x, y)}(dx^2 + dy^2),$$

where $\lambda : S \rightarrow R$ is a smooth scalar function defined on the surface, the so called conformal factor.

The Ricci flow is the process to deform the metric $\mathbf{g}(t)$ according to its induced Gaussian curvature $K(t)$, where t is the time parameter, such that the curvature evolves according to a non-linear heat diffusion process:

$$\frac{dg_{ij}(t)}{dt} = -2K(t)g_{ij}(t). \quad (2)$$

with the constraint that the total surface area is preserved. Let $\mathbf{g}(t) = e^{2u(t)}\mathbf{g}(0)$.

The Ricci flow is

$$\frac{du(t)}{dt} = -2K(t), \quad (3)$$

At any time t , the metric $\mathbf{g}(t)$ is conformal to the original metric $\mathbf{g}(0)$. The Ricci flow can be easily modified to compute a metric with a prescribed curvature \bar{K} , and then the flow becomes

$$\frac{dg_{ij}(t)}{dt} = 2(\bar{K} - K(t))g_{ij}(t). \quad (4)$$

The goal here is to find a conformal mapping to map the surface to a circle domain, so we set the target curvature for interior points to be 0, and the boundary geodesic curvature to be constant.

Discrete Surface Ricci Flow. The discrete surface Ricci flow is the exact analogy of the smooth surface Ricci flow. A surface is approximated by piecewise linear triangular mesh $M = (V, E, F)$. The discrete Riemannian metric is represented by the edge lengths, the discrete Gaussian curvature is formulated as angle deficit,

$$K(v_i) = \begin{cases} 2\pi - \sum_{jk} \theta_i^{jk}, & \forall v_i \notin \partial M \\ \pi - \sum_{jk} \theta_i^{jk}, & \forall v_i \in \partial M \end{cases} \quad (5)$$

where θ_i^{jk} is the corner angle at the vertex v_i in the face $[v_i, v_j, v_k]$. The total discrete curvature satisfies the Gauss-Bonnet theorem, $\sum_{v_i \in M} K(v_i) = 2\pi\chi(M)$, where $\chi(M)$ is the Euler characteristic number of the mesh M .

We associate each vertex v_i with a circle $c(v_i, \gamma_i)$, the circles associated with the two end vertices of an edge $[v_i, v_j]$ intersect at an angle ϕ_{ij} . The edge length is given by

$$l_{ij} = \sqrt{\gamma_i^2 + \gamma_j^2 + 2\gamma_i\gamma_j \cos \phi_{ij}}, \quad (6)$$

which is called the circle packing metric. We then deform the discrete metric by changing the circle radii $\{\gamma_i\}$'s, but preserving the circle intersection angles $\{\phi_{ij}\}$'s. The *discrete conformal factor* is given by $u_i = \log \gamma_i$, then the *discrete surface Ricci flow* has the same formula as the smooth counter part, $du_i/dt = \bar{K}_i - K_i$. The discrete surface Ricci flow is the gradient flow of the convex energy

$$E(\mathbf{u}) = \int_{\mathbf{u}_0}^{\mathbf{u}_n} \sum_{i=1}^n (\bar{K}_i - K_i) du_i,$$

therefore, the flow converges to the unique global optimum. The convex energy can be efficiently optimized using Newton's method. The computational details are as follows: for each face $[v_i, v_j, v_k]$, there is a unique circle orthogonal to 3 circles $c(v_i, \gamma_i)$, $c(v_j, \gamma_j)$ and $c(v_k, \gamma_k)$, which is called the power circle of the face. Each edge $e \in M$ is shared by two faces, we connect the power centers of the two faces to get the dual edge of e , denoted as \bar{e} , then we obtain the dual

mesh \bar{M} . Given an edge e_{ij} connecting v_i and v_j , we define the *edge weight* on it $w_{ij} = |\bar{e}_{ij}|/|e_{ij}|$, where $|\bar{e}_{ij}|$ is the length of the dual edge. The Hessian matrix $\mathbf{H} = (\partial^2 E(\mathbf{u})/\partial u_i \partial u_j)$ is given by

$$\frac{\partial^2 E(\mathbf{u})}{\partial u_i \partial u_j} = \begin{cases} -w_{ij}, & v_i \sim v_j \\ \sum_{k \neq i} w_{ik}, & i = j \\ 0, & v_i \not\sim v_j \end{cases} \quad (7)$$

The gradient of the energy is given by

$$\nabla E(\mathbf{u}) = (\bar{K}_1 - K_1, \bar{K}_2 - K_2, \dots, \bar{K}_n - K_n)^T. \quad (8)$$

In the Newton's method, at each step, the change of conformal factor $\delta \mathbf{u}$ satisfies the equation: $H(\mathbf{u})\delta \mathbf{u} = \nabla E(\mathbf{u})$.

The target curvatures are subtle. The total curvature of exterior boundary vertices is 2π , for each interior boundaries, the total curvature is -2π . Fix one interior boundary, suppose the vertices are consecutively labeled as $\{v_0, v_1, \dots, v_{k-1}\}$, then the target curvature should satisfy $\sum_i \bar{K}(v_i) = -2\pi$,

$$\frac{\bar{K}(v_i)}{|\bar{e}_{i-1,i}| + |\bar{e}_{i,i+1}|} = \text{const},$$

where the edge lengths are the target edge length, which are unknown at the beginning. Hence, the algorithm iteratively updates the target curvatures of the boundary vertices.

The *power distance* from a point p on the surface to the vertex v_i is given by $\text{Pow}(p, v_i) = |p - v_i|^2 - \gamma_i^2$. The *power voronoi diagram* of the mesh is a cell decomposition, $S = \bigcup_i W_i$, where each cell $W_i := \{p \in S \mid \text{Pow}(p, v_i) \leq \text{Pow}(p, v_j)\}$.

The *power Delaunay* triangulation is the dual to the power voronoi diagram. During the whole flow, the triangulation is maintained to be power Delaunay by edge swap operations. This can ensure the existence of the solution to arbitrary target curvature $\bar{K} : V \rightarrow R$, if $\bar{K}(v_i) \in (-\infty, 2\pi)$ and $\sum_i \bar{K}(v_i) = 2\pi\chi(M)$. Detailed proof can be found in [44].

2.2. Discrete Optimal Mass Transport

Suppose μ has compact support on X , define $\Omega = \text{Supp}\mu = \{x \in X | \mu(x) > 0\}$, assume Ω is a convex domain in X . The space Y is discretized to $Y = \langle y_1, y_2, \dots, y_n \rangle$ with Dirac measure $\nu = \sum_{j=1}^n \nu_j \delta(y - y_j)$.

We define a height vector $\mathbf{h} = (h_1, h_2, \dots, h_n) \in \mathbb{R}^n$, consisting of n real numbers. For each $y_i \in Y$, we construct a hyperplane defined on X : $\pi_i(\mathbf{h}) : \langle x, y_i \rangle + h_i = 0$, where $\langle \cdot, \cdot \rangle$ is the inner product in \mathbb{R}^n . Define a function: $u_{\mathbf{h}}(x) = \max_i \{\langle x, y_i \rangle + h_i\}$, then $f(\mathbf{h}, x)$ is a convex function. We denote its graph by $G(\mathbf{h})$, which is an infinite convex polyhedron with supporting planes $\pi_i(\mathbf{h})$. The projection of $G(\mathbf{h})$ induces a polygonal partition of Ω , $\Omega = \bigcup_{i=1}^n W_i(\mathbf{h})$, and $W_i(\mathbf{h}) = \{x \in X | u_{\mathbf{h}}(x) = \langle x, y_i \rangle + h_i\} \cap \Omega$. Each cell $W_i(\mathbf{h})$ is the projection of a facet of the convex polyhedron $G(\mathbf{h})$ onto Ω . The convex function $u_{\mathbf{h}}$ on each cell $W_i(\mathbf{h})$ is a linear function $\pi_i(\mathbf{h})$, therefore, the gradient map

$$\text{grad } u_{\mathbf{h}} : W_i(\mathbf{h}) \rightarrow y_i, i = 1, 2, \dots, n. \quad (9)$$

maps each $W_i(\mathbf{h})$ to a single point y_i . The following theorem plays a fundamental role here:

Theorem 1. *For any given measure $\mu, \nu_j > 0, j = 1, \dots, n$, such that $\sum_{j=1}^n \nu_j = \int_{\Omega} \mu$, there must exist a height vector \mathbf{h} unique up to adding a constant vector (c, c, \dots, c) , the convex function $u_{\mathbf{h}}$ induces the cell decomposition of Ω , such that the following area-preservation constraints are satisfied for all cells,*

$$\int_{W_i(\mathbf{h})} \mu(x) dx = \nu_i, i = 1, 2, \dots, n. \quad (10)$$

Furthermore, the gradient map $\text{grad } u_{\mathbf{h}}$ optimizes the following transportation cost

$$E(T) := \int_{\Omega} |x - T(x)|^2 \mu(x) dx. \quad (11)$$

The existence and uniqueness have been first proven by Alexandrov using a topological method [45]. The existence has been also proven by Aurenhammer, Hoffmann and Aronov [46], and the uniqueness and optimality have been proven by Brenier (see for instance [47], Theorem 2.12(ii), and Theorem 2.32).

Recently, Gu et al. [17] have given a novel proof for the existence and uniqueness based on variational principle. The global minimum can be obtained efficiently using Newton's method.

First, we define the admissible space of the height vectors:

$$H_0 := \left\{ \mathbf{h} \mid \int_{W_i(\mathbf{h})} \mu > 0, \sum_i h_i = 0 \right\}.$$

Then, define the energy $E(\mathbf{h})$ as the volume of the convex polyhedron bounded by the graph $G(\mathbf{h})$ and the cylinder through Ω minus a linear term,

$$E(\mathbf{h}) = \int_{\Omega} u_{\mathbf{h}}(x) \mu(x) dx - \sum_{i=1}^n \nu_i h_i. \quad (12)$$

The gradient of the energy is given by:

$$\nabla E(\mathbf{h}) = \left(\int_{W_i(\mathbf{h})} \mu(x) dx - \nu_i \right), \quad (13)$$

Suppose the cells $W_i(\mathbf{h})$ and $W_j(\mathbf{h})$ intersect at an edge $e_{ij} = W_i(\mathbf{h}) \cap W_j(\mathbf{h}) \cap \Omega$, then the Hessian matrix of $E(\mathbf{h})$ is given by:

$$\frac{\partial^2 E(\mathbf{h})}{\partial h_i \partial h_j} = \begin{cases} \frac{1}{|y_j - y_i|} \int_{e_{ij}} \mu & , \quad W_i(\mathbf{h}) \cap W_j(\mathbf{h}) \cap \Omega \\ 0 & , \quad otherwise. \end{cases} \quad (14)$$

In Gu et al. [17], it is proven that H_0 is convex, and the Hessian is positive definite on H_0 , the global unique minimum \mathbf{h} is an interior point of H_0 . At the minimum point, the gradient map $grad u_{\mathbf{h}}$ meets the measure-preserving constraints in Eqn. 10. Furthermore, this gradient map is the optimal mass transportation map.

3. Algorithm

This section explains the details of the computational algorithms.

3.1. Conformal Mapping Using Ricci Flow to Planar Poly Annulus

The first stage is to compute the conformal mapping, the surface is mapped onto a planar circle domain. By initializing the parameterization by a conformal

mapping is helpful to reduce the angle distortion of the final area-preserving mapping as explained in [7]. The conformal parameterization method based on holomorphic 1-forms [22] is equivalent to the geometric Finite Element Method. The quality of the triangle meshes will affect the convergence and accuracy of the algorithm. In contrast, Ricci flow method has no requirement to the triangle mesh quality, the existence and uniqueness of the solution are guaranteed in theory [44]. Therefore, in the current work, we adopt the Ricci flow method.

Suppose the input triangle mesh $M = (V, E, F)$ is given.

1. Compute the Initial Circle Packing Metric

First, we compute the circum center of each face $[v_i, v_j, v_k]$, the circum radius is denoted as d_{ijk} . Then for each vertex v_i , we define its circle radius γ_i as

$$\gamma_i = \min_{jk} d_{ijk}.$$

Set the discrete conformal factor $u_i = \log \gamma_i, i = 1, 2, \dots, n$.

Second, we initialize the intersection angles for circles associated with two end vertices of an edge. Consider edge $[v_i, v_j]$, we use the circle packing metric formula Eqn. 6 to compute the value of $\cos \phi_{ij}$.

2. Compute the Initial Target Curvature

For all interior vertex $v \notin \partial M$, its target curvature is set to be 0, $\bar{K}(v) \leftarrow 0$. Trace the boundary loops, denoted as $\Gamma_0, \Gamma_1, \dots, \Gamma_m$. The Γ_0 is the exterior boundary. $|\Gamma_i|$ denotes the number of vertices in $\Gamma_i, i = 1, \dots, m$. For any vertex on $v_k \in \Gamma_0$, its target Gaussian curvature is

$$\bar{K}_k \leftarrow \frac{2\pi}{|\Gamma_0|}, k = 1, \dots, |\Gamma_0|.$$

For any vertex on $v_k \in \Gamma_i, i \neq 0$, its target Gaussian curvature is

$$\bar{K}_k \leftarrow -\frac{2\pi}{|\Gamma_i|}, k = 1, \dots, |\Gamma_i|.$$

3. Newton's Method

From the current conformal factor, compute the edge lengths

$$l_{ij} = \sqrt{e^{2u_i} + e^{2u_j} + 2e^{u_i}e^{u_j} \cos \phi_{ij}},$$

update the triangulation to be Power Delaunay by edge swapping. From the edge length, compute the corner angles

$$\theta_i^{jk} \leftarrow \cos^{-1} \frac{l_{ij}^2 + l_{ki}^2 - l_{jk}^2}{2l_{ij}l_{ki}},$$

from the corner angles to compute the vertex curvatures $K(v_i)$ using Eqn. 5. Compute the gradient of the entropy energy $\nabla E(\mathbf{u})$ using Eqn. 8. Compute the power circle for each face, compute edge weight w_{ij} for each edge, construct the Hessian matrix of entropy energy using formula Eqn. 7. Solve the positive definite linear system

$$H(\mathbf{u})\delta\mathbf{u} = \nabla E(\mathbf{u}),$$

with the constraint $\sum_i u_i = 0$, using conjugate gradient method. Update the discrete conformal factor

$$\mathbf{u} \leftarrow \mathbf{u} + \epsilon \delta \mathbf{u},$$

where ϵ is the step length.

Repeat the whole procedure, until the curvature error is less than a given threshold

$$\max_i |\bar{K}_i - K_i| < \text{threshold},$$

4. Update the Boundary Target Curvature

Suppose Γ_0 is represented as a list of consecutive vertices $\{v_0, \dots, v_{k-1}, v_k, v_{k+1}, \dots\}$, compute the total length of Γ_0

$$s_0 = \sum_{v_k \in \Gamma_0} l_{k-1,k},$$

update the target curvature as

$$\bar{K}(v_k) = 2\pi \frac{l_{k-1,k} + l_{k,k+1}}{2s_0}$$

Similarly, consider an interior boundary loop Γ_i ,

$$s_i = \sum_{v_k \in \Gamma_i} l_{k-1,k},$$

update the target curvature for $v_k \in \Gamma_i$ as

$$\bar{K}(v_k) = -2\pi \frac{l_{k-1,k} + l_{k,k+1}}{2s_i}.$$

5. Iteration

Repeat step 3 and 4, until the change of the target curvatures on boundary vertices are all less than a given threshold. We denote the conformal mapping obtained in this stage as $\varphi : M \rightarrow \Omega$, where Ω is a circle domain contained in the planar unit disk, $\Omega = \mathbb{D} \setminus B(p_i, r_i)$, where $B(p_i, r_i)$ is a disk centered at p_i with radius r_i .

3.2. Optimal Mass Transportation Map

In the second stage, we compute the optimal transportation map.

Initialization of Target Area. We use the conformal mapping result to set up the target domain and the target measure,

$$D := \{(\varphi(v_1), a\mu_1), (\varphi(v_2), a\mu_2), \dots, (\varphi(v_n), a\mu_n)\} \bigcup_{i=1}^m \{(p_i, b\nu_i)\},$$

where $\varphi(v_k)$ is the conformal mapping image of vertex v_k ,

$$\mu_k := \frac{1}{3} \sum_{jk} \text{Area}([v_i, v_j, v_k]),$$

where μ_k is the Dirac measure associated with $\varphi(v_k)$, which is the one third of the total area of the faces attached to it in the mesh in \mathbb{R}^3 . p_i is the center of the i -th circular hole of the circle domain, ν_i is the area of the hole $\nu_i = \pi r_i^2$. Positive constants $a, b > 0$ are used to normalize the total area, and the relative sizes of the holes

$$a \sum_{k=1}^n \mu_k + b \sum_{i=1}^m \nu_i = \pi.$$

Optimal Mass Transport Mapping. For the convenience of discussion, we rewrite the target as

$$D = \{(y_1, \bar{w}_1), (y_2, \bar{w}_2), \dots, (y_{n+m}, \bar{w}_{n+m})\}.$$

We plan to compute the unique optimal mass transportation $\tau : \mathbb{D} \rightarrow \{(y_i, \bar{w}_i)\}$. According to the Monge-Briener theory, we need to find the height vector $\mathbf{h} = (h_1, h_2, \dots, h_{n+m})$. Fix a height vector, the support planes are given by $\{\pi_i(\mathbf{h}) : \langle x, y_i \rangle + h_i\}$, the convex function is $u_{\mathbf{h}}(x) = \max_i \langle x, y_i \rangle + h_i$, and its

graph $G(\mathbf{h})$ can be computed as upper envelope of the supporting plane $\pi_i(\mathbf{h})$. The projection of $G(\mathbf{h})$ onto \mathbb{D} forms a polygonal partition $\mathbb{D} = \bigcup_i W_i(\mathbf{h})$. The algorithm is as follows:

1. Initialize the height

$$h_i = -\frac{1}{2}\langle y_i, y_i \rangle, i = 1, 2, \dots, n+m,$$

2. Compute the upper envelope of the planes $\{\pi_i\}$'s, which is equivalent to compute the power voronoi diagram of the unit disk

$$\mathbb{D} = \bigcup_{i=1}^{n+m} W_i(\mathbf{h}),$$

the area of each cell is denoted as

$$w_i(\mathbf{h}) = \text{Area}(W_i(\mathbf{h})).$$

Then we compute the dual power Delaunay triangulation.

3. The Hessian matrix is given by $H(\mathbf{h}) = (h_{ij}(\mathbf{h}))$,

$$h_{ij}(\mathbf{h}) = \begin{cases} -|\tilde{e}_{ij}|/|e_{ij}|, & i \neq j, W_i \cap W_j \cap \mathbb{D} \neq \emptyset \\ \sum_{k \neq i} h_{ik}, & i = j \\ 0, & \text{otherwise} \end{cases}$$

where $|e_{ij}|$ is the length of the dual power Delaunay triangulation edge and $|\tilde{e}_{ij}|$ is the length of power voronoi diagram edge.

4. Solve the linear system using conjugate gradient method

$$H(\mathbf{h})\delta\mathbf{h} = \bar{\mathbf{w}} - \mathbf{w},$$

with the constraint $\sum_i h_i \bar{w}_i = 0$. Then we update the height vector

$$\mathbf{h} \leftarrow \mathbf{h} + \epsilon \delta\mathbf{h},$$

where ϵ is a step length parameter.

5. Repeat step 2 through 4, until

$$\max_i |\bar{w}_i - w_i(\mathbf{h})| < \text{threshold}.$$

4. Experimental Results

In this section, we demonstrate the efficiency and efficacy of our method using examples from the real world.

All the experiments were conducted on a laptop computer of Intel Core i5-4200U CPU, 2.29GHz with 8GB memory. All the algorithms are implemented using generic C++ with visual studio 2013 on Windows 10 platform.

4.1. Area-preserving Parameterization

Fig. 2 illustrates our area-preserving parameterization result. The semi-world-cup model in frame (a) is a genus zero surface with three boundaries. We conformally map it onto a circle domain using Ricci flow method as shown in frame (b). The conformal mapping produces large area distortions near the lid region, which is zoomed in frame (c). Then, we compute the optimal mass transportation mapping to obtain the area-preserving parameterization as shown in frame (d), where the area distortions are within the threshold prescribed by users, as demonstrated in the zoomed image in frame (e).

Fig. 3 further compares angle-preserving and area-preserving parameterizations. We slice the genus one surface model along two fundamental group generators to make it a genus zero surface with one boundary, then we punch three holes as shown in frame (a) and (b). The poly annulus is conformally mapped onto a circle domain as shown in frame (c) using Ricci flow, then the circle domain is further mapped using OMT to obtain the area-preserving parameterization as shown in frame (d). By comparing frame (c) and (d), we can see the ear regions have large distortions in (c), and the area elements are well preserved in (d).

4.2. Texture Mapping

Fig. 4 demonstrates a direct application of our OMT parameterization: area-preserving texture mapping. In order to show the flexibility of our method, we test it on surfaces with different topologies. All the surfaces in the figure are of genus 0, but with different number of boundaries. Our method is general

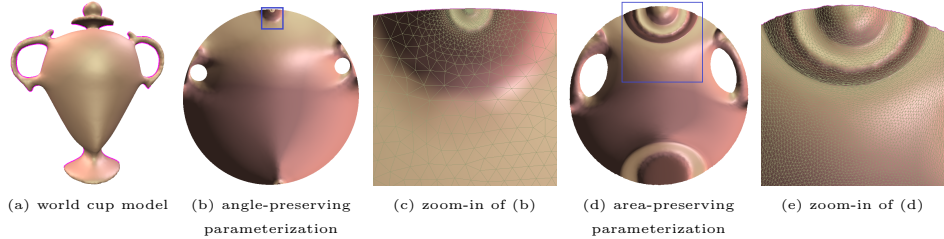


Figure 2: Comparison between angle-preserving and area-preserving parameterizations. It is obvious that the angle-preserving parameterization induces large area distortions in the lid region; in contrast, the area-preserving parameterization almost eliminates the area distortions.

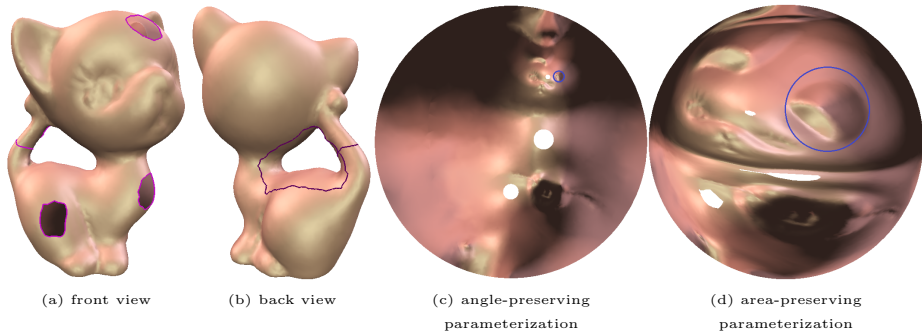


Figure 3: Comparison between angle-preserving and area-preserving parameterizations for the sliced kitten model. It is easy to see that the angle-preserving parameterization induces large area distortions in the kitten ear regions (c), the area-preserving parameterization avoids area distortion thoroughly (d).

enough to handle arbitrary topological poly annuli without any modification or adaption. In order to visualize the correspondence between the texture and the surface, we use a checker board texture with numerical labels, such that the users can easily locate each checker on the geometric surface. It can be easily verified that all the checkers on the surface are with similar areas.

Fig. 5 compares the conformal texture mapping and the area-preserving texture mapping. The conformal texture mapping results are shown in the first and the third columns, which preserve the local shapes well but distort the area undesirably; in contrast, the area-preserving results are shown in the 2nd and the 4th columns, which preserve the areas but distort the local shapes. Depending on the real applications, user may prefer different texture mapping

method, or combine both of them for visualization purpose.

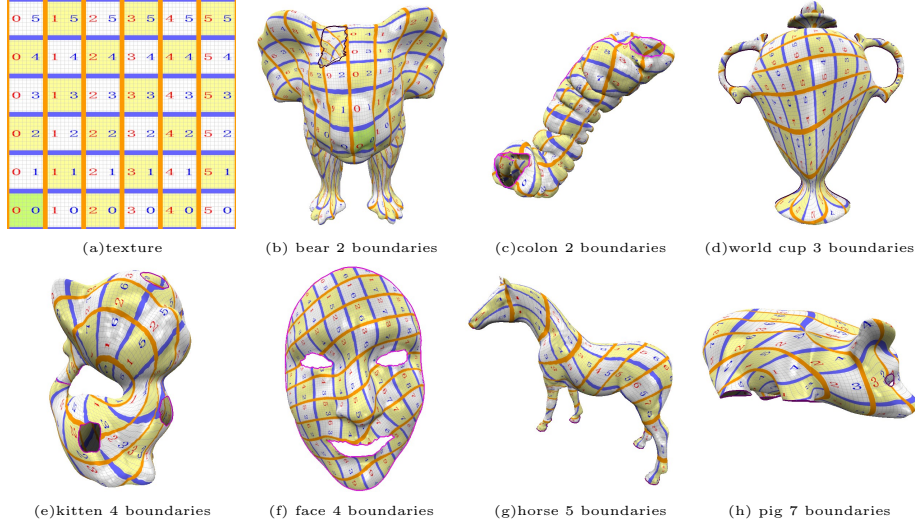


Figure 4: Area-preserving texture mapping for poly annuli. Our method is general enough to handle genus zero surfaces with arbitrary number of boundaries.

4.3. Importance driven Surface Parameterization

Our method allows users to fully control the texture area of regions of interests. By adjusting the target measure, the user can zoom or shrink specific regions on the surface as shown in Fig. 6 and 7. The top row demonstrates that the user can control the areas of the holes, the bottom row shows the user can enlarge/shrink the nose region with different scaling factors in 6. The similar visual effect is also achieved for the skull model as shown in 7.

4.4. Evaluation

Area-Preserving. In order to quantify the parameterization quality, we compute the distribution of the area-distortion factor explicitly as follows: for each face on the mesh, we calculate the ratio between its 3D geometric area and 2D parameter area, then we compute the histogram of the area-distortion factors and shown in Fig. 8 Frame (a) shows the histogram of area-distortion factors of OMT parameterization of the human face model, (b) the histogram produced

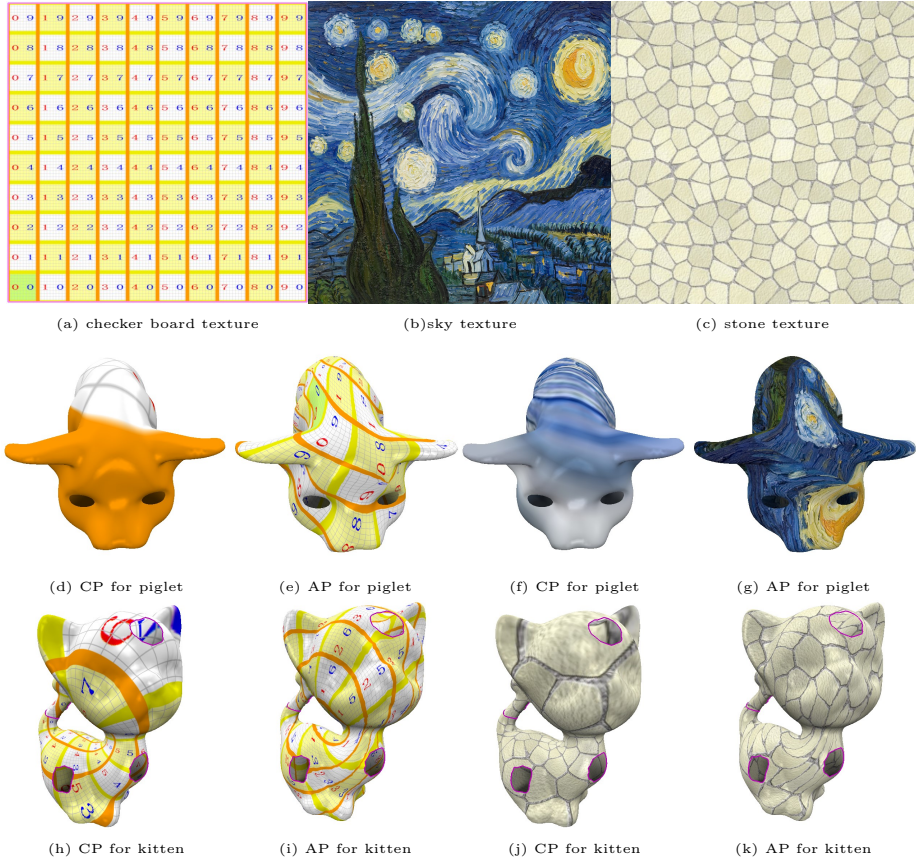


Figure 5: Comparison of area-preserving and conformal texture mapping; (a)-(c) image used as texture; (d)-(g) texture mapping results for piglet model; (h)-(k) texture mapping results for sliced kitten model. 'CF' is the conformal texture mapping. 'AP' stands for area-preserving texture mapping.

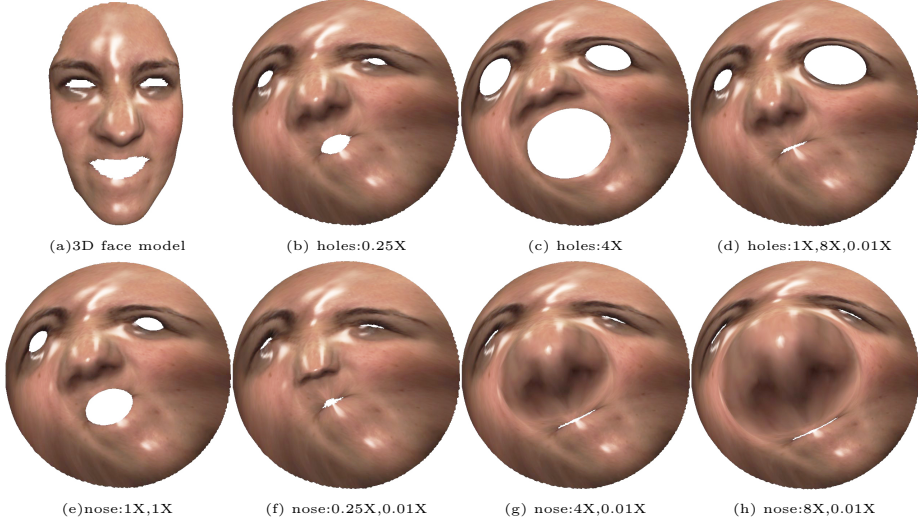


Figure 6: Importance driven surface parameterization for a human face; (a) the 3d face model; (b)-(d) shows importance driven results of the holes with different scaling factors; (e)-(h) shows the importance driven results of the nose and holes with different scaling factors.

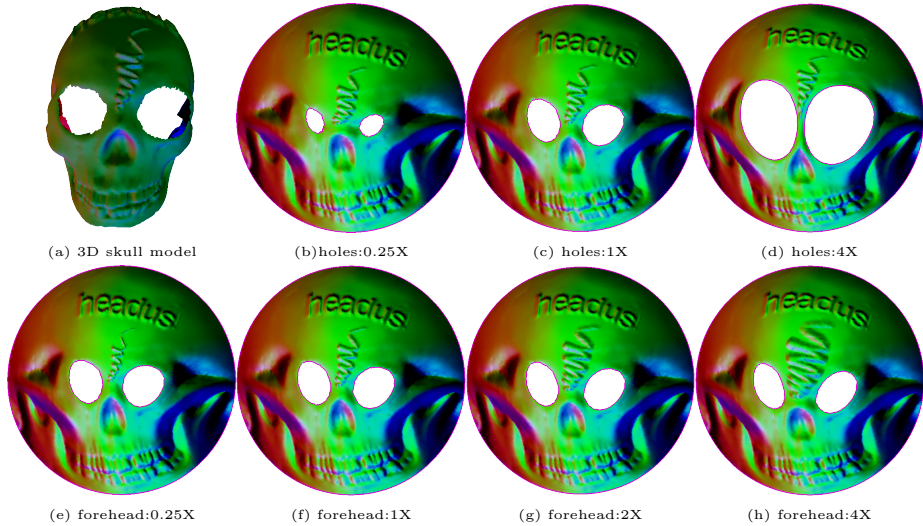


Figure 7: Importance driven surface parameterization for the skull model; (a) the 3D skull model; (b)-(d) shows importance driven results of the holes with different scaling factors; (e)-(h) shows the importance driven results of the forehead region with different scaling factors.

by the conformal parametrization of the same face model. It is obvious that the histogram produced by OMT parameterization highly concentrates near the origin, namely, the mapping result is highly area-preserving. On the contrary, the histogram induced by Ricci flow is widely distributed. Similarly, we compare the histograms for the Piglet model in frame (c) and (d), which further verifies the fact that our OMT based method achieves higher accuracy.

Robustness and Efficiency. We verify the robustness of our method by testing it on meshes with complicated topologies, as shown in Fig. 4. We deliberately modify the topologies of the surfaces to challenge our algorithm. In practice, our method can smoothly handle all of them without any modification or adaption, which demonstrates that our method is robust to complicated topologies.

We test the performance of our algorithm and report the statistics in Table 1, where the number of faces of the models, the iterations and the running time are summarized. We can see for meshes with high geometric complexity (55k faces), high topological complexity (7 boundaries), the running time is less than 2 minutes, without any optimization of our implementation. We compare the area distortion and angle distortion induced by different parameterization algorithms on different models, as shown in Fig. 8.

Table 1: Performance Statistics

Model	boundaries	faces	number of iterations		time in minutes	
			error < 1e-6	error < 1e-12	error < 1e-6	error < 1e-12
Bear,fig4.(b)	2	46852	56	83	1.012	1.587
World-cup,fig4.(c)	3	24035	101	127	0.993	1.282
Colon,fig4.(d)	2	18203	240	266	1.718	1.957
Kitten,fig4.(e)	4	20090	42	64	0.341	0.524
Face,fig4.(f)	4	39465	17	43	0.312	0.767
Horse,fig4.(g)	5	39622	54	81	0.836	1.298
Piglet,fig4.(h)	7	55203	118	145	1.752	1.969

In addition, we compare our algorithm with alternative quasi-area preserving method, such as stretch minimization parameterization [15]. We demonstrate our area-preserving method and quasi-area preserving method on four typical mesh models which are topologically equivalent to the unit disk, since the quasi-area preserving can not handle complex topology. Fig. 9 compares the

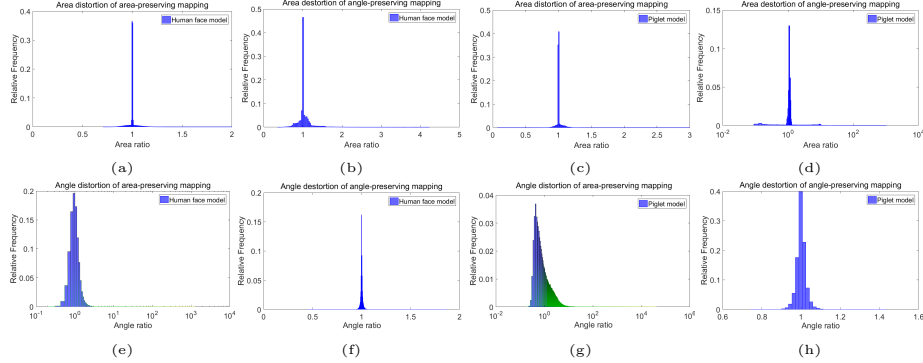


Figure 8: Comparison between histograms of the area and angle distortion; (a) area distortion of OMT for the human face model; (b) area distortion of conformal mapping for the human face model; (c) area distortion of OMT for the piglet model; (d) area distortion of conformal mapping for the piglet model; (e) angle distortion of OMT for the human face model; (f) angle distortion of conformal mapping for the human face model; (g) angle distortion of OMT for the piglet model; (h) angle distortion of conformal mapping for the piglet model.

histograms of the area distortion of our method (orange) and stretch minimization method (blue). It is obvious that the histogram of our method is highly concentrated around 1, while that of stretch minimization method is widely spread. The distortion statistics are shown in Table 2. This shows our method achieves much higher quality in terms of area preserving. On the other hand, our method is highly non-linear and is more time consuming, about 1.5 times slower as shown in Table 2.

Table 2: Performance Statistics

Model	# vertices	# faces	time in seconds		max		average		std	
			OMT	Quasi	OMT	Quasi	OMT	Quasi	OMT	Quasi
Bear Head	13768	27370	6.666	8.717	1.7692	8.1893	1.0011	0.9117	0.0358	0.2635
Alex	21326	42184	7.97	4.399	1.5387	3.3272	1.004	1.0014	0.0436	0.0874
Terrain	51902	102771	32.869	20.235	3.0725	4.6912	1.0010	0.9977	0.0375	0.2046
Venus	10430	20754	4.261	3.342	4.6486	2.8708	1.0025	0.9997	0.0547	0.4157

5. Conclusion

This work proposes a novel parameterization method, based on discrete surface Ricci flow and optimal mass transportation theories. The algorithm

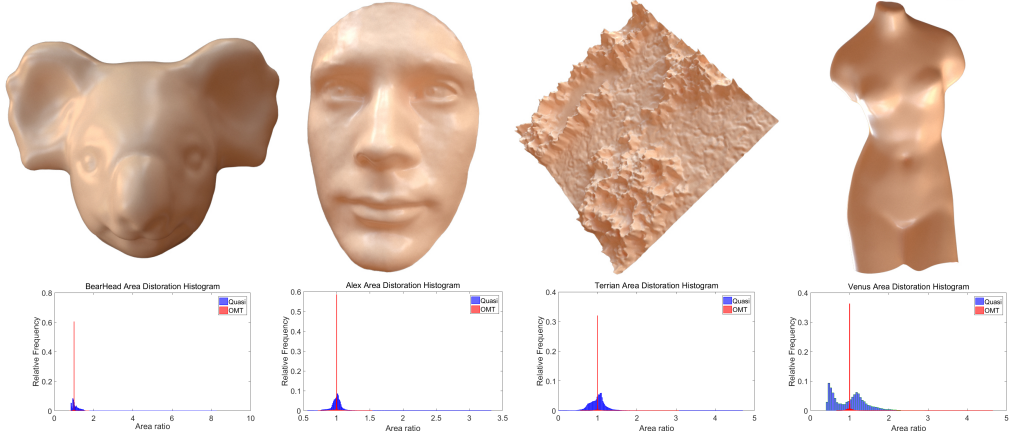


Figure 9: The first row is the bear head, Alex face, terrain and Venus mesh model; The second row shows the comparison between the histograms of area distortions induced by OMT method and the stretch minimization method.

is capable of finding area-preserving parameterizations for genus zero surfaces with multiple boundaries. The achieved mapping is diffeomorphic and invariant under conformal transformations. Conventional Kontarovich’s approach has $O(n^2)$ unknown variables, whereas the proposed method has only $O(n)$ variables, where n is the number of vertices on the mesh. Furthermore, the algorithm gives users full control of the area of each part on the texture domain. Both Ricci flow and Optimal Mass Transport Map are based on convex optimizations. Our experimental results demonstrate the efficiency and efficacy of the proposed method. In practice, conformal mapping and area-preserving mapping have different advantages and disadvantages. Depending on the real applications, users can choose one of them or a combination of them.

In future, we will explore the way to generalize the current framework to high genus surfaces, and find more applications in various engineering and medical fields.

6. Acknowledgement

This work was supported by National Natural Science Foundation (Grant Nos. DMS-1418255, DMS-1221339), AFOSR FA9550-10-1-0294, AFOSR FA955014-

1-0193 and National Natural Science Foundation of China (Grant No. 61328206, No. 11271156, No. 11001017). The authors are also grateful to anonymous referees for their helpful comments and suggestions.

References

References

- [1] K. Hormann, K. Polthier, A. Sheffer, Mesh parameterization: theory and practice, in: ACM SIGGRAPH ASIA 2008 courses, ACM, 2008, p. 12.
- [2] A. Sheffer, K. Hormann, B. Lévy, M. Desbrun, K. Zhou, E. Praun, H. Hoppe, Mesh parameterization: theory and practice, ACM SIGGRAPH 2007 course notes (2007).
- [3] A. Sheffer, E. Praun, K. Rose, Mesh parameterization methods and their applications, Foundations and Trends® in Computer Graphics and Vision 2 (2) (2006) 105–171.
- [4] M. S. Floater, M. Reimers, Meshless parameterization and surface reconstruction, Computer Aided Geometric Design 18 (2) (2001) 77–92.
- [5] M. S. Floater, K. Hormann, M. Reimers, Parameterization of manifold triangulations, in: Approximation Theory X: Abstract and Classical Analysis, Vanderbilt University Press, Nashville, 2002, pp. 197–209.
- [6] L. Zhang, L. Liu, C. Gotsman, H. Huang, Mesh reconstruction by meshless denoising and parameterization, Computers & Graphics 34 (3) (2010) 198–208.
- [7] A. Dominitz, A. Tannenbaum, Texture mapping via optimal mass transport, IEEE Transactions on Visualization and Computer Graphics 16 (3) (2010) 419–433.
- [8] B. Lévy, J.-L. Mallet, Non-distorted texture mapping for sheared triangulated meshes, in: Proceedings of the 25th annual conference on Computer graphics and interactive techniques, ACM, 1998, pp. 343–352.

- [9] B. Lévy, S. Petitjean, N. Ray, J. Maillot, Least squares conformal maps for automatic texture atlas generation, *ACM Transactions on Graphics (TOG)* 21 (3) (2002) 362–371.
- [10] L. Liu, L. Zhang, Y. Xu, C. Gotsman, S. J. Gortler, A local/global approach to mesh parameterization, *Computer Graphics Forum* 27 (5) (2008) 1495–1504.
- [11] A. Sheffer, B. Lévy, M. Mogilnitsky, A. Bogomyakov, ABF++: fast and robust angle based flattening, *ACM Transactions on Graphics (TOG)* 24 (2) (2005) 311–330.
- [12] M. S. Floater, Parametrization and smooth approximation of surface triangulations, *Computer aided geometric design* 14 (3) (1997) 231–250.
- [13] M. S. Floater, K. Hormann, Surface parameterization: a tutorial and survey, *Advances in multiresolution for geometric modelling* (2005) 157–186.
- [14] A. Sheffer, E. D. Sturler, Surface parameterization for meshing by triangulation flattening, in: Proc. 9th International Meshing Roundtable, 2000, pp. 161–172.
- [15] S. Yoshizawa, A. Belaev, H.-P. Seidel, A fast and simple stretch-minimizing mesh parameterization, in: *Shape Modeling Applications 2004*, IEEE, 2004, pp. 200–208.
- [16] G. Zou, J. Hu, X. Gu, J. Hua, Authalic parameterization of general surfaces using lie advection, *IEEE Transactions on Visualization and Computer Graphics* 17 (12) (2011) 2005–2014.
- [17] X. Gu, F. Luo, J. Sun, S.-T. Yau, Variational principles for Minkowski type problems, discrete optimal transport, and discrete Monge-Ampère equations, *Asian Journal of Mathematics(AJM)* 2 (20) (2016) 383–398.
- [18] L. Kantorovich, On a problem of Monge, *Uspekhi Mat. Nauk.* 3 (1948) 225–226.

- [19] Y. Brenier, Polar factorization and monotone rearrangement of vector-valued functions, *Communications on pure and applied mathematics* 44 (4) (1991) 375–417.
- [20] B. Chow, F. Luo, Combinatorial Ricci flow on surfaces, *Journal Differential Geometry* 61 (1) (2003) 97–129.
- [21] M. Desbrun, M. Meyer, P. Alliez, Intrinsic parameterizations of surface meshes, *Computer Graphics Forum* 21 (3) (2002) 209–218.
- [22] X. Gu, S.-T. Yau, Global conformal surface parameterization, in: *Proceedings of the 2003 Eurographics/ACM SIGGRAPH Symposium on Geometry processing*, Eurographics Association, 2003, pp. 127–137.
- [23] K. Hormann, G. Greiner, S. Campagna, Hierarchical parametrization of triangulated surfaces, in: *Vision, Modeling, and Visualization*, Vol. 1999, 1999, p. 219.
- [24] A. Sheffer, E. de Sturler, Parameterization of faceted surfaces for meshing using angle-based flattening, *Engineering with Computers* 17 (3) (2001) 326–337.
- [25] B. Springborn, P. Schröder, U. Pinkall, Conformal equivalence of triangle meshes, *ACM Transactions on Graphics (TOG)* 27 (3) (2008) 77.
- [26] M. Jin, J. Kim, F. Luo, X. Gu, Discrete surface Ricci flow, *IEEE Transactions on Visualization and Computer Graphics* 14 (5) (2008) 1030–1043.
- [27] K. Crane, U. Pinkall, P. Schröder, Spin transformations of discrete surfaces, *ACM Transactions on Graphics (TOG)* 30 (4) (2011) 104.
- [28] C. Schüller, L. Kavan, D. Panozzo, O. Sorkine-Hornung, Locally injective mappings, *Computer Graphics Forum* 32 (5) (2013) 125–135.
- [29] Z. Levi, D. Zorin, Strict minimizers for geometric optimization, *ACM Transactions on Graphics (TOG)* 33 (6) (2014) 185.

- [30] Y. Lipman, Bounded distortion mapping spaces for triangular meshes, *ACM Transactions on Graphics (TOG)* 31 (4) (2012) 108.
- [31] N. Aigerman, Y. Lipman, Injective and bounded distortion mappings in 3d, *ACM Transactions on Graphics (TOG)* 32 (4) (2013) 106.
- [32] S. Z. Kovalsky, N. Aigerman, R. Basri, Y. Lipman, Controlling singular values with semidefinite programming, *ACM Transactions on Graphics (TOG)* 33 (4) (2014) 68–1.
- [33] S. Z. Kovalsky, N. Aigerman, R. Basri, Y. Lipman, Large-scale bounded distortion mappings, *ACM Transactions on Graphics (TOG)* 34 (6) (2015) 191.
- [34] L. Zhu, S. Haker, A. Tannenbaum, *Area-preserving mappings for the visualization of medical structures*, Springer, 2003.
- [35] S. Haker, L. Zhu, A. Tannenbaum, S. Angenent, Optimal mass transport for registration and warping, *International Journal of computer vision* 60 (3) (2004) 225–240.
- [36] T. ur Rehman, E. Haber, G. Pryor, J. Melonakos, A. Tannenbaum, 3D non-rigid registration via optimal mass transport on the GPU, *Medical image analysis* 13 (6) (2009) 931–940.
- [37] X. Zhao, Z. Su, X. D. Gu, A. Kaufman, J. Sun, J. Gao, F. Luo, Area-preservation mapping using optimal mass transport, *IEEE Transactions on Visualization and Computer Graphics* 19 (12) (2013) 2838–2847.
- [38] Q. Mérigot, A multiscale approach to optimal transport, *Computer Graphics Forum* 30 (5) (2011) 1583–1592.
- [39] F. De Goes, D. Cohen-Steiner, P. Alliez, M. Desbrun, An optimal transport approach to robust reconstruction and simplification of 2d shapes, in: *Eurographics Symposium on Geometry Processing*, Vol. 30, 2011, pp. 1593–1602.

- [40] F. de Goes, K. Breeden, V. Ostromoukhov, M. Desbrun, Blue noise through optimal transport, ACM Transactions on Graphics (TOG) 31 (6) (2012) 171.
- [41] W. Zeng, X. D. Gu, Ricci flow for shape analysis and surface registration: theories, algorithms and applications, Springer Science & Business Media, 2013.
- [42] Y. Wang, X. Gu, T. F. Chan, P. M. Thompson, S.-T. Yau, Brain surface conformal parameterization with the Ricci flow, IEEE Trans. Med. Imag. 31 (2) (2012) 251–264.
- [43] W. Zeng, X. Yin, M. Zhang, F. Luo, X. Gu, Generalized Koebe’s method for conformal mapping multiply connected domains, in: 2009 SIAM/ACM Joint Conference on Geometric and Physical Modeling, ACM, 2009, pp. 89–100.
- [44] X. Gu, F. Luo, J. Sun, T. Wu, A discrete uniformization theorem for polyhedral surfaces, arXiv:1309.4175 (2013).
- [45] A. D. Alexandrov, Convex polyhedra, translated from the 1950 russian edition Edition, Springer Monographs in Mathematics, Springer-Verlag, Berlin, 2005.
- [46] F. Aurenhammer, F. Hoffmann, B. Aronov, Minkowski-type theorems and least-squares clustering, Algorithmica 20 (1) (1998) 61–76.
- [47] C. Villani, Topics in optimal transportation, no. 58 in Graduate Studies in Mathematics, American Mathematical Society, Providence, RI, 2003.